

2023

## Memory-based adaptive sliding mode load frequency control in interconnected power systems with energy storage

Farhad Farivar  
*Edith Cowan University*

Octavian Bass  
*Edith Cowan University*

Daryoush Habibi  
*Edith Cowan University*

Follow this and additional works at: <https://ro.ecu.edu.au/ecuworks2022-2026>



Part of the [Electrical and Computer Engineering Commons](#)

---

10.1109/ACCESS.2023.3317181

Farivar, F., Bass, O., & Habibi, D. (2023). Memory-based adaptive sliding mode load frequency control in interconnected power systems with energy storage. *IEEE Access*, 11, 102515-102530. <https://doi.org/10.1109/ACCESS.2023.3317181>

This Journal Article is posted at Research Online.  
<https://ro.ecu.edu.au/ecuworks2022-2026/3101>

Received 26 July 2023, accepted 13 September 2023, date of publication 19 September 2023,  
date of current version 25 September 2023.

Digital Object Identifier 10.1109/ACCESS.2023.3317181

## RESEARCH ARTICLE

# Memory-Based Adaptive Sliding Mode Load Frequency Control in Interconnected Power Systems With Energy Storage

FARHAD FARIVAR<sup>1</sup>, (Graduate Student Member, IEEE),  
OCTAVIAN BASS<sup>1</sup>, (Senior Member, IEEE), AND DARYOUSH HABIBI<sup>1</sup>, (Senior Member, IEEE)

School of Engineering, Edith Cowan University (ECU), Joondalup, Perth, WA 6027, Australia

Corresponding author: Farhad Farivar (f.farivar@ecu.edu.au)

**ABSTRACT** This paper presents a memory-based adaptive sliding mode load frequency control (LFC) strategy aimed at minimizing the impacts of exogenous power disturbances and parameter uncertainties on frequency deviations in interconnected power systems with energy storage. First, the dynamic model of the system is constructed by considering the participation of the energy storage system (ESS) in the conventional decentralized LFC model of a multiarea power system. A disturbance observer (DOB) is proposed to generate an online approximation of the lumped disturbance. In order to enhance the transient performance of the system and effectively mitigate the adverse effects of power fluctuations on grid frequency, a novel memory-based sliding surface is developed. This sliding surface incorporates the estimation of the lumped disturbance, as well as the past and present information of the state variables. The conservative assumption about the lumped disturbance is eased by considering the unknown upper bound of the disturbance and its first derivative. Based on the output of the proposed DOB, an adaptive continuous sliding mode controller with prescribed  $H_\infty$  performance index is introduced. This controller ensures that the sliding surface is reachable and guarantees asymptotic stability of the closed-loop system. The controller design utilizes strict linear matrix inequalities (LMIs) to achieve these objectives. Finally, the applicability and efficacy of the proposed scheme are verified through comparative simulation cases.

**INDEX TERMS** Disturbance estimation error, disturbance observer, energy storage system, memory-based sliding mode load frequency control, robustness.

## I. INTRODUCTION

LOAD frequency control (LFC) is an integral part of automatic generation control as it aims to maintain frequency fluctuations within an acceptable range [1]. It is evident that continuous frequency deviations in power systems can result in transmission line overloads, malfunctioning of power system protection equipment and severe damage to frequency-sensitive devices [2]. However, in recent years, the introduction of intermittent renewable generators, such as solar and wind power, along with complex load patterns, unknown system dynamics and variations in system parameters, has introduced additional uncertainties to power systems

[3]. Consequently, the performance of existing conventional PI-based frequency controllers in thermal generation units has been inadequate in meeting grid requirements [4]. For these reasons, the suitability of fast-response ancillary frequency regulation services has recently been explored for the LFC problem to ensure the reliable operation of power system. For example, the deployment of energy storage system (ESS) such as battery energy storage system and superconducting magnetic storage system, has recently been under investigation as a means to address the LFC problem [5]. Nevertheless, the widespread utilization of these storage devices is not practical due to design complexities, coupled with high costs associated with installation and maintenance [6]. Other alternative approaches, such as distributed control load and pumped storage power plants,

The associate editor coordinating the review of this manuscript and approving it for publication was Xiaosong Hu<sup>1</sup>.

TABLE 1. List of Symbols.

Symbol	Variables
$i$	$i$ th area of the power system
$j$	$j$ th area of the power system
$\Delta f_i$	Frequency deviation (Hz)
$\Delta X_{G_i}$	Variation in position of governor valve (p.u.MW)
$\Delta M_{G_i}$	Generator power deviation (p.u.MW)
$\Delta P_{L_i}$	Load disturbance (p.u.MW)
$\Delta P_{WT_i}$	Wind turbine output power fluctuation (p.u.MW)
$\Delta T_i$	Deviation in tie-line active power (p.u.MW)
$\Delta P_{B_i}$	Energy storage power deviation (p.u.MW)
$T_{P_i}$	Power system time constant (sec)
$T_{T_i}$	Turbine time constant (sec)
$T_{G_i}$	Governor time constant (sec)
$K_{P_i}$	Power system gain (Hz/p.u.MW)
$q_{ij}$	Tie-line interconnection gain between area $i$ and $j$ (p.u.MW/rad/sec)
$\alpha_i$	Thermal power plant participation factor for area $i$
$\chi_i$	Energy storage system participation factor for area $i$
$R_i$	Droop coefficient (Hz/p.u.MW)
$B^\dagger$	Pseudo inverse of matrix $B$
*	Transposed elements of a symmetrical matrix
GRC	Generation rate constraint p.u.MW/sec
GDB	Governor deadband
LMI	Linear matrix inequality
DOB	Disturbance observer
PI	Proportional integral
SMC	Sliding mode control
SMLFC	Sliding mode load frequency control
MASMLFC	Memory-based adaptive sliding mode load frequency control

have also been introduced. However, the effectiveness of these approaches is influenced by power system uncertainties [7]. Hence, it is crucial to employ more efficient and practical control strategies within existing structures to ensure that frequency deviations in interconnected power systems are maintained within specified limits. To tackle power system uncertainties associated with the LFC problem, enhanced control schemes have been introduced, such as evolutionary and meta-heuristic based PI controllers [8], model predictive control [9], adaptive control [10], fuzzy control [11], artificial neural network control [12], optimal control [13],  $H_\infty$  control [14], [15], sliding mode control (SMC) [16], [17], active disturbance rejection controller [18] and event-triggered load frequency control [19], [20]. Additional comparative discussions regarding the effectiveness of various frequency control methods can be found in [21], [22].

Among these control techniques, the SMC scheme has garnered significant attention in various industrial applications [23], [24], particularly in power system frequency control. This is due to its robustness in handling unmodeled system dynamics, parameter variations and disturbance attenuation [25], [26], [27]. In recent years, the LFC problem in inter-linked power grids has encountered additional challenges due to disturbances arising from complex load patterns and renewable resources like wind power. These challenges have led to difficulties where the governor of generation units fails to adequately respond to frequency deviations [28], [29]. Accordingly, these disturbances fall under the category of mismatched disturbances, which are introduced into the system through a different channel than the control input. As a result, they can impact the inherent robustness of traditional sliding mode controllers. To tackle the issue of

mismatched disturbances, integral-based SMC schemes have been introduced. These schemes aim to preserve the complete robustness properties of traditional SMC against mismatched external disturbances [30], [31]. The authors of [32], [33], [34] investigated the LFC problem in power systems with both load disturbances and system parameter variations, considering lumping together all mismatched and matched disturbances to maintain the robustness property of traditional SMC. However, these approaches were constrained by assumptions made regarding the rank of the disturbance matrix. In addition, none of these works incorporated an optimal method to determine the sliding mode controller gains, which are essential for ensuring the asymptotic stability of the state variables within a finite time. Moreover, it is well-known that the performance of the control system can be affected by integral action, often leading to large overshoot and long settling time. Additionally, the utilization of a discontinuous term in the integral-based sliding surface in the proposed controllers has been shown to lead to a degradation in the performance of the sliding surface. This degradation was primarily due to the high-frequency chattering behavior exhibited by the sliding surface function. To address this chattering problem, some researchers have incorporated a disturbance observer (DOB) in the design of SMC, as described in [35], [36]. However, these methods have been limited to systems with matched disturbances. The DOB-SMC approaches proposed in [37], [38] demonstrated favorable performance against mismatched external disturbances. Nevertheless, these controllers were designed under the restrictive assumption of known disturbance boundaries, whereby the controller gains were selected conservatively and without utilizing any optimal algorithm. A thorough examination of DOB controllers can be found in [39]. In [28], the authors have proposed an adaptive higher order terminal sliding mode LFC method. In their work, an adaptive control law was employed to approximate the upper bound of external disturbances. In [40], an intelligence-based terminal sliding mode approach with ESS integration for the LFC problem was proposed. However, the applicability of the proposed scheme was not tested for power systems experiencing mismatched disturbances from intermittent renewable generators. Similarly, the adaptive method described in [41] did not investigate the influence of external disturbances originating from renewable energy resources. In contrast, the fuzzy-SMC method presented in [7] focused on the LFC problem in power systems that incorporate both wind power and ESS. The frequency controller gains were tuned using an imperialistic competitive algorithm, whereby a seamless approximation function was proposed to mitigate the chattering problem commonly associated with sliding mode control. In [42] a higher-order SMC method was constructed based on a super-twisting algorithm combined with a disturbance observer. The gains of the controller were determined using a linear quadratic regulator scheme, providing robustness against system uncertainties. However, the effectiveness of this approach was constrained to the

tracking of step load disturbances exclusively. The approach in [43] introduced a sliding mode controller for the LFC problem with extensive integration of electric vehicles. In this scheme, the disturbance boundaries were assumed to be known values, and a chattering-free sliding surface was proposed. The controller gains were determined using particle swarm optimization. However, it is worth noting here that the robustness of the controller was not evaluated against the adverse effects of renewable energy power disturbances. The authors of [44] introduced a fractional-order integral sliding mode based on an extended disturbance observer. The impacts of energy storage system and wind power generation on power system frequency deviation were studied. The superiority of the proposed approach in terms of control performance was demonstrated when compared to conventional integer-order controllers.

Based on the preceding discussion, it appears that the  $H_\infty$  performance criteria have not been addressed explicitly in the SMC controller design to minimize the impact of external disturbance on controlled output (frequency deviations). Furthermore, it is important to note that, to the best of our knowledge, the transient performance of the proposed sliding mode controllers has not been directly addressed in a wide range of industrial applications, including the LFC problem in interlinked power grids. In this paper, a novel memory-based adaptive sliding mode frequency controller is proposed to address the LFC problem in multi-area interconnected power systems, in collaboration with an ESS acting as an auxiliary frequency regulation device. Motivated from the above discussion, the main contributions of this work are summarized as follows:

- A disturbance observer is proposed to estimate the disturbances caused by power fluctuations, load changes and variations in system parameters. The output of the disturbance observer is then integrated into the sliding surface design to mitigate the chattering problem, and to compensate for the impact of the aforementioned disturbances on frequency deviations.
- The introduction of a memory-based sliding surface, which incorporates past information of state variables, improves the transient performance of the control system compared to other methods [45]. Furthermore, an additional enhancement in the frequency deviation response is accomplished by utilizing an ancillary energy storage system for frequency regulation.
- A continuous control law is developed to guarantee the global stability of the closed-loop system and to alleviate the chattering problem for practical implementations.
- Unlike conventional approaches [46], [47], an adaptive law is derived in the controller without requiring predetermined values of the upper limit of the lumped disturbance boundary.
- To minimize the impact of both matched and mismatched disturbances on frequency deviations, the controller design introduces a guaranteed  $H_\infty$  performance using strict LMIs.

The subsequent sections of this paper are structured as follows. Section II provides the descriptions of the system dynamic model. Section III presents the design of the Disturbance Observer (DOB) and the synthesis of the proposed adaptive sliding mode load frequency controller. Simulation results are illustrated in Section IV. Finally, Section V concludes the paper and explores the potential for future work.

## II. DESCRIPTION OF THE SYSTEM MODEL

While a multiarea interconnected power system is inherently nonlinear, the linearized model is commonly used for LFC studies. This is mainly due to the assumption that slow variations in loads and generation resources occur under normal operational conditions [1], [3]. Based on the conventional decentralized LFC model described in [42], [48], the block diagram representing the  $i$ th area of a multiarea power system is depicted in Fig. 1. Therefore, the effectiveness of the LFC strategy primarily relies on the accuracy of the system model, which considers power perturbations. The various system components are modeled as follows.

### A. MODELING WIND POWER FLUCTUATIONS

In this study, the fluctuations in wind turbine output power  $\Delta P_{WT}(t)$  are considered as renewable power disturbances that do not contribute to frequency regulation. The output mechanical power of the wind turbine can be determined using the following expression [49], [50]:

$$P_{WTi} = \frac{1}{2} \rho_{wi} A_{wr} C_{wp} (\lambda_{wi}, \beta_{wi}) V_{wi}^3 \quad (1)$$

$$C_{wp} = (0.44 - 0.0167\beta_{wi}) \sin\left(\frac{\pi(\lambda_{wi} - 3)}{15 - 0.3\beta_{wi}}\right) - 0.0184(\lambda_{wi} - 3)\beta_{wi} \quad (2)$$

where  $\lambda_{wi} = \frac{R_{blade}\omega_{blade}}{V_{wi}}$ ,  $\rho_w$ ,  $A_{wr}$ ,  $C_{wp}$ ,  $\lambda_w$ ,  $\beta_w$ ,  $V_{wi}$ ,  $R_{blade}$  and  $\omega_{blade}$  are the air density ( $kg/m^3$ ), the effective area of the blades ( $m^2$ ), power coefficient, tip speed ratio, blade pitch angle, wind speed ( $m/s$ ) blade radius and the blade rotational speed, respectively.

### B. MODELING ENERGY STORAGE SYSTEM

The ESS serves as a fast-response auxiliary frequency regulation device, enhancing the dynamic response of the power system to frequency deviations and alleviating transient stress on traditional thermal power plants [49]. As the ESS requires time to control its charge and discharge, a first-order lag model is employed to study the LFC problem in hybrid power systems [50]. The first-order lag model is represented by the following equation:

$$G_{ESS}(s) = \frac{K_{B_i}}{1 + sT_{B_i}} \quad (3)$$

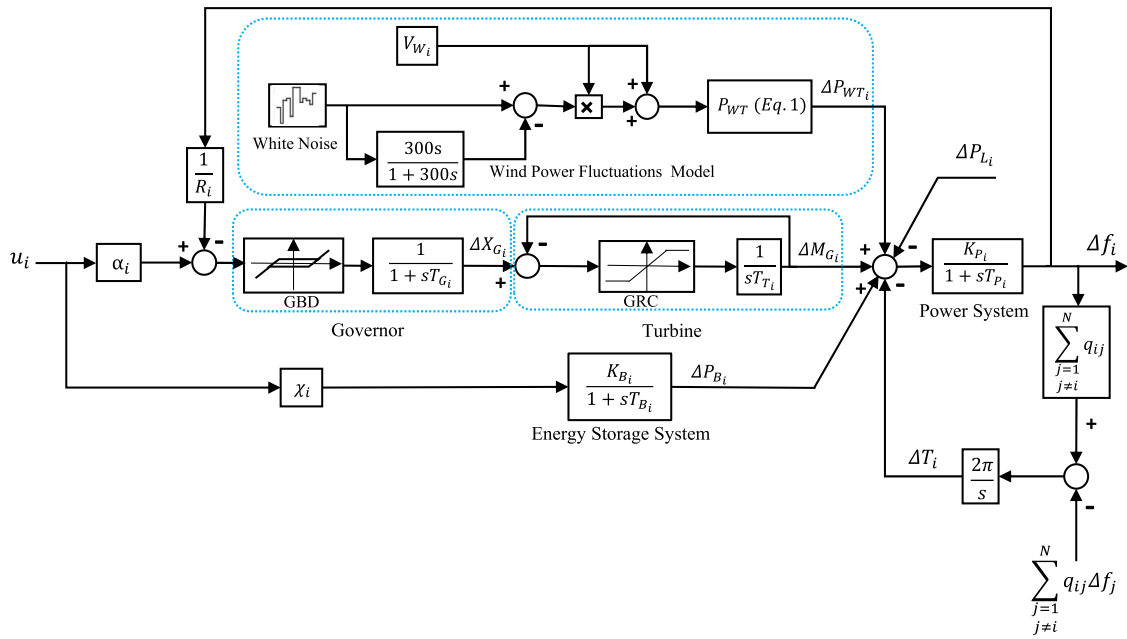


FIGURE 1. Power system LFC structure for the *i*th area of multi-area power system.

The variable gain  $K_{B_i}$  in the system is influenced by the state of charge (SOC) of the energy storage device. Further details for optimal calculation of  $K_{B_i}$  can be found in [41].

C. MODELING MULTIAREA POWER SYSTEM

As mentioned in the introduction section, the primary objective of the LFC system is to ensure a suitable response from the generator side to power disturbances originating from load variations, tie-line fluctuations and intermittent renewable sources. Thus, the total external disturbance for the *i*th area can be defined as  $W_i(t) = \Delta P_{WT_i}(t) - \Delta P_{L_i}(t) - \Delta T_i(t)$  [42], [48].

Assumption 1: The total external perturbation  $W_i(t)$  is bounded, satisfying  $\|W_i(t)\| \leq \epsilon_i$ , where  $\epsilon_i$  represents a positive constant.

In view of the above definition, the state space equations of the system dynamics for the *i*th area of the interconnected power system shown in Fig. 1 are described as follows:

$$\Delta \dot{f}_i(t) = -\frac{1}{T_{P_i}(t)} \Delta f_i(t) + \frac{K_{P_i}}{T_{P_i}(t)} \Delta P_{B_i}(t) + \frac{K_{P_i}}{T_{P_i}(t)} \Delta M_{G_i}(t) - \frac{K_{P_i}}{T_{P_i}(t)} W_i(t) \quad (4)$$

$$\Delta \dot{P}_{B_i}(t) = -\frac{1}{T_{B_i}(t)} \Delta P_{B_i}(t) + \frac{K_{B_i}}{T_{B_i}(t)} \delta_i u_i(t) \quad (5)$$

$$\Delta \dot{M}_{G_i}(t) = -\frac{1}{T_{T_i}(t)} \Delta M_{G_i}(t) + \frac{1}{T_{T_i}(t)} \Delta X_{G_i}(t) \quad (6)$$

$$\Delta \dot{X}_{G_i}(t) = -\frac{1}{T_{G_i}(t)} \Delta X_{G_i}(t) - \frac{1}{R_i T_{G_i}(t)} \Delta f_i(t) + \frac{1}{T_{G_i}(t)} \alpha_i u_i(t) \quad (7)$$

$$y_i(t) = \Delta f_i(t) \quad (8)$$

(4)–(8) can be described by the following matrix form:

$$\begin{aligned} \dot{x}_i(t) &= A_i(t)x_i(t) + B_i(t)u_i(t) + F_i(t)W_i(t) \\ y_i(t) &= C_i x_i(t) \end{aligned} \quad (9)$$

In the provided equation,  $A_i(t)$ ,  $B_i(t)$ ,  $F_i(t)$  and  $C_i$  represent real system matrices with appropriate dimensions. The state vector is given by  $x_i(t) = [\Delta f_i(t) \quad \Delta P_{B_i}(t) \quad \Delta M_{G_i}(t) \quad \Delta X_{G_i}(t)]^T$ , where  $x_i(t) \in R^n(t)$ . The control input is denoted as  $u_i(t) \in R$ .  $W_i(t)$  represents the total external disturbance, and  $y_i(t)$  corresponds to the controlled output (frequency deviation).

$$\begin{aligned} A_i(t) &= \begin{bmatrix} -\frac{1}{T_{P_i}(t)} & \frac{K_{P_i}}{T_{P_i}(t)} & \frac{K_{P_i}}{T_{P_i}(t)} & 0 \\ 0 & -\frac{1}{T_{B_i}(t)} & 0 & 0 \\ 0 & 0 & -\frac{1}{T_{T_i}(t)} & \frac{1}{T_{T_i}(t)} \\ -\frac{1}{R_i T_{G_i}(t)} & 0 & 0 & -\frac{1}{T_{G_i}(t)} \end{bmatrix} \\ B_i(t) &= \begin{bmatrix} 0 & \frac{\delta_i K_{B_i}}{T_{B_i}(t)} & 0 & \frac{\alpha_i}{T_{G_i}(t)} \end{bmatrix}^T \\ F_i(t) &= \begin{bmatrix} -\frac{K_{P_i}}{T_{P_i}(t)} & 0 & 0 & 0 \end{bmatrix}^T \\ C_i &= \begin{bmatrix} 1 & 0 & 0 & 0 \end{bmatrix} \end{aligned}$$

Considering the uncertainties in power system parameters, the system state space form (9) can be represented in a nominal and bounded uncertainty form as follows:

$$\begin{aligned} \dot{x}_i(t) &= (A_i + \Delta A_i(t))x_i(t) + (B_i + \Delta B_i(t))u_i(t) \\ &\quad + (F_i + \Delta F_i(t))W_i(t) \end{aligned} \quad (10)$$

As both the total external disturbance  $W_i(t)$  and system uncertainties are bounded, we can infer from the (10) that

$$\dot{x}_i(t) = A_i x_i(t) + B_i u_i(t) + f_i(t) \quad (11)$$

where  $f_i(t)$  is defined as the lumped disturbance, given by

$$f_i(t) = \Delta A_i(t)x_i(t) + \Delta B_i(t)u_i(t) + (F_i + \Delta F_i(t))W_i(t) \quad (12)$$

*Assumption 2:* The lumped disturbance  $f_i(t)$  and its first derivative  $\dot{f}_i(t)$  satisfy  $\|f_i(t)\| \leq \theta_{1i}$  and  $\|\dot{f}_i(t)\| \leq \theta_{2i}$ , where  $\theta_{1i}$  and  $\theta_{2i}$  are positive constants.

### III. DESIGN OF THE PROPOSED SLIDING MODE LFC SCHEME

This section illustrates the design of the memory-based sliding mode controller via a DOB for the LFC problem. The structure of the intended controller is given in Fig. 2.

#### A. DISTURBANCE OBSERVER DESIGN

The disturbance observer is proposed as follows:

$$\begin{aligned} \dot{z}_i(t) &= -L_i(z_i(t) + L_i x_i(t)) - L_i(A_i x_i(t) + B_i u_i(t)) \\ \hat{f}_i(t) &= z_i(t) + L_i x_i(t) \end{aligned} \quad (13)$$

where  $z_i$  denotes the state space vector of the observer,  $\hat{d}_i(t)$  is the lumped disturbance estimation in (11) and  $L_i$  is a positive definite matrix. The lumped disturbance estimation error is defined as  $e_{d_i}(t) = \hat{f}_i(t) - f_i(t)$ . The boundedness of  $e_{d_i}(t)$  is proved with the aid of following lemmas.

*Lemma 1* ([59]): Consider the following system

$$\dot{\eta} = f_i(\eta, u) \quad (14)$$

where  $f_i(\eta, u)$  is locally Lipschitz;  $u$  is bounded and exhibits piecewise continuity. If the unforced form of (14) possesses a globally exponentially stable equilibrium point at the origin, then the system (14) exhibits input-to-state stability (ISS).

*Lemma 2:* For a given disturbance observer (13), the disturbance estimation error  $e_{d_i}(t) = \hat{f}_i(t) - f_i(t)$  satisfies  $\|e_{d_i}(t)\| \leq n_i$ , where  $n_i$  is a positive constant.

*Proof:* Combining (11) into (13), we obtain

$$\begin{aligned} \dot{e}_{d_i}(t) &= (\dot{z}_i(t) + L_i \dot{x}_i(t)) - \dot{f}_i(t) \\ &= -L_i(\hat{f}_i(t) - f_i(t)) - \dot{f}_i(t) \\ &= -L_i e_{d_i}(t) - \dot{f}_i(t) \end{aligned} \quad (15)$$

Since  $L_i$  is an arbitrary positive definite matrix, then the unforced form of system (15) with  $\dot{f}_i(t) = 0$  has a globally exponentially stable equilibrium point at the origin. By taking Assumption 2,  $\dot{f}_i(t)$  is considered as a bounded signal, and recalling Lemma 1, the system (15) becomes ISS, meaning that the disturbance estimation error  $e_{d_i}(t)$  tends to zero. This completes the proof. ■

Further details to determine the scalar  $n_i$  can be found in [60], which can be determined as

$$n_i = c_i \theta_{1i} - c_i \theta_{2i} \frac{2}{n_{\max}(L_i)}. \quad (16)$$

#### B. THE SYNTHESIS OF THE MEMORY-BASED ADAPTIVE SMC

In this subsection, we design a memory-based SMC scheme that: ensures the global stability of the system dynamics in (11); minimizes the impact of the lumped disturbance  $f_i(t)$  on the controlled output; and improves the transient performance of the controller. To meet these requirements, we construct a controller with  $H_\infty$  performance based on the following criteria:

- 1) The system dynamics in (11) with  $f_i(t) = 0$  are globally asymptotically stable.
- 2) For a given positive scalar  $\gamma_i$ ,  $f_i(t) \neq 0$  and  $f_i(t) \in \mathcal{L}_2[0, +\infty)$ , the following inequality holds under zero initial condition

$$\int_0^\infty \|y_i(t)\|^2 dt \leq \gamma_i^2 \int_0^\infty \|f_i(t)\|^2 dt \quad (17)$$

We consider the following memory-based sliding surface:

$$\begin{aligned} s_i(t) &= H_i(x_i(t) - x_i(0)) \\ &\quad - \int_0^t (A_i x_i(v) + B_i u_{s_i}(v) + \hat{f}_i(v)) dv \end{aligned} \quad (18)$$

where  $H_i \in R^{m \times n}$  is the disturbance attenuation gain to be selected in a way that  $H_i B_i$  becomes a non-singular matrix,  $u_{s_i}(t) = K_i x_i(t) - K_{\tau_i} x_i(t - \tau_i) - H_i \hat{f}_i(t)$ , in which  $K_i$  and  $K_{\tau_i}$  are the controller gains, and  $\tau_i$  is the memory parameter.

*Remark 1:* The practical advantage of the sliding surface (18) compared to conventional integral sliding surfaces [31] is its utilization of the estimated lumped disturbance  $\hat{f}_i(t)$ . This allows for active minimization of the effects of power disturbances arising from load variations and wind power fluctuations on the frequency deviations.

*Remark 2:* Compared to the conventional integral sliding surfaces in [37], [43], the proposed memory-based sliding surface (18) incorporates a memory parameter to retain and utilize delayed information of the state variables. Thus,  $u_{s_i}$  in (18) can be rewritten as  $u_{s_i}(t) = \bar{K}_i x_i(t) - \bar{K}_{\tau_i} \frac{x_i(t) - x_i(t - \tau_i)}{\tau_i} - H_i \hat{f}_i(t)$ , where  $\bar{K}_i = K_i + \tau_i K_{\tau_i}$  and  $\bar{K}_{\tau_i} = \tau_i K_{\tau_i}$ . Noticing that  $\dot{x}_i(t) \approx \frac{x_i(t) - x_i(t - \tau_i)}{\tau_i}$ , it is observed that the memory-based sliding surface (18) includes the derivative control term. Based on the PID control theory, the inclusion of a derivative control action can enhance the transient performance of the control system. Therefore, by incorporating a memory-based SMC scheme, it is expected to achieve superior transient performance. This will be validated through the simulation results.

The next theorem shows that the reachability of sliding mode dynamics in (18) onto the sliding surface will be guaranteed.

*Theorem 1:* Let us consider the sliding surface  $s_i(t)$  in (18), assuming that  $\theta_{1i}$ ,  $\theta_{2i}$ ,  $K_i$  and  $K_{\tau_i}$  are known parameters. The sliding mode dynamics will reach into a region around the sliding surface in finite time by designing the control laws as follows:

$$u_i(t) = u_{s_i}(t) + H_i u_{r_i}(t)$$

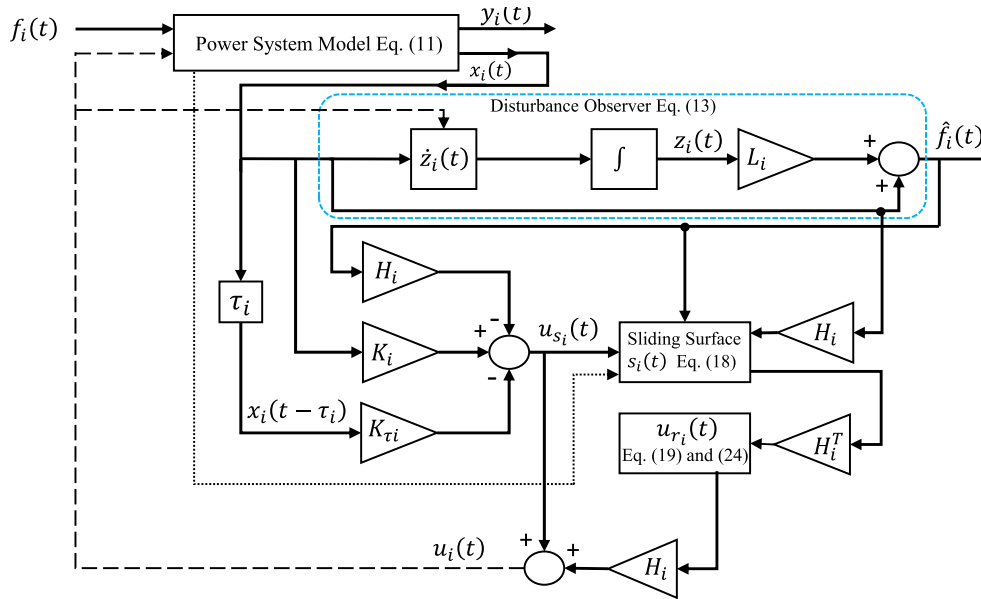


FIGURE 2. Control diagram of the proposed memory-based sliding mode controller with disturbance observer.

$$u_{r_i}(t) = -(m_i + n_i) \text{sat} \left( H_i^T s_i(t) \right), \quad m_i > 0 \quad (19)$$

where  $u_{s_i}$  and  $n_i$  were defined in (18) and (16), and

$$\text{sat}(H_i^T s_i(t)) = \begin{cases} \frac{H_i^T s_i(t)}{\delta_i}, & \|H_i^T s_i(t)\| < \delta_i \\ \frac{H_i^T s_i(t)}{\|H_i^T s_i(t)\|}, & \|H_i^T s_i(t)\| \geq \delta_i \end{cases}$$

*Proof:* Let's select the Lyapunov candidate function  $V_i(t) = \frac{1}{2} s_i^T(t) (H_i B_i)^{-1} s_i(t)$ . Taking the derivative of  $V_i(t)$  along with time yields

$$\begin{aligned} \dot{V}_i(t) &= s_i^T(t) (H_i B_i)^{-1} \dot{s}_i(t) \\ &= s_i^T(t) (H_i B_i)^{-1} \left( H_i (\dot{x}_i(t) - A_i x_i(t) - B_i u_{s_i}(t) - \hat{f}_i(t)) \right) \\ &= s_i^T(t) (H_i B_i)^{-1} \left( H_i (B_i (u_i(t) - u_{s_i}(t)) + f_i(t) - \hat{f}_i(t)) \right) \\ &= s_i^T(t) (u_i(t) - u_{s_i}(t)) + s_i^T(t) (H_i B_i)^{-1} H_i (f_i(t) - \hat{f}_i(t)) \end{aligned} \quad (20)$$

Let  $H_i = B_i^\dagger$ , then  $(H_i B_i)^{-1}$  becomes an identity matrix. Substituting the control law in (19) into (20),  $\dot{V}_i(t)$  can be rewritten as

$$\begin{aligned} \dot{V}_i(t) &= s_i^T(t) H_i u_{r_i}(t) + s_i^T(t) H_i (f_i(t) - \hat{f}_i(t)) \\ &= s_i^T(t) H_i (u_{r_i}(t) - e_{d_i}(t)) \\ &= s_i^T(t) H_i \left( -(m_i + n_i) \text{sat} \left( H_i^T s_i(t) \right) - e_{d_i}(t) \right) \end{aligned} \quad (21)$$

If  $\|H_i^T s_i(t)\| \geq \delta_i$ , it can be verified from (21) that

$$\begin{aligned} \dot{V}_i(t) &= -(m_i + n_i) \|H_i^T s_i(t)\| - s_i^T(t) H_i e_{d_i}(t) \\ &\leq -m_i \|H_i^T s_i(t)\| \end{aligned} \quad (22)$$

If  $\|H_i^T s_i(t)\| < \delta_i$ , it is obtained from (21) that

$$\begin{aligned} \dot{V}_i(t) &\leq -(m_i + n_i) \frac{\|H_i^T s_i(t)\|^2}{\delta_i} + \|H_i^T s_i(t)\| n_i \\ &= -m_i \frac{\|H_i^T s_i(t)\|^2}{\delta_i} + \frac{n_i}{\delta_i} \left( \|H_i^T s_i(t)\| \delta_i \right. \\ &\quad \left. - \|H_i^T s_i(t)\|^2 \right) \end{aligned} \quad (23)$$

Based on (22) and (23), there exists a scalar  $m_i$  such that  $\dot{V}_i(t) \leq 0$ , which means that the state trajectories can be kept on the sliding region via the proposed controller. Hence, the proof is completed. ■

*Corollary 1:* Suppose that  $\theta_{1i}$  and  $\theta_{2i}$  are unknown scalars. The sliding mode dynamics will reach into a region around the sliding surface (18) in finite time by proposing the following adaptive control law:

$$\begin{aligned} u_i(t) &= u_{s_i}(t) + H_i u_{r_i}(t) \\ u_{r_i}(t) &= -(m_i + \hat{n}_i) \text{sat} \left( H_i^T s_i(t) \right), \quad m_i > 0. \end{aligned} \quad (24)$$

where  $\hat{n}_i$  is the adaptive law, which is designed as

$$\dot{\hat{n}}_i = \kappa_i \|H_i^T s_i(t)\|, \quad \kappa_i > 0. \quad (25)$$

*Proof:* By defining  $\tilde{n}_i(t) = n_i(t) - \hat{n}_i(t)$  and considering the Lyapunov function as  $V(t) = \frac{1}{2} \left( s_i^T(t) s_i(t) + \frac{1}{\kappa_i} \tilde{n}_i^2(t) \right)$ , we can readily obtain

$$\begin{aligned} \dot{V}(t) &= s_i^T(t) \dot{s}_i(t) - \frac{1}{\kappa_i} \tilde{n}_i(t) \dot{\hat{n}}_i \\ &= s_i^T(t) \left( -H_i (m_i + \hat{n}_i(t)) \text{sat} \left( H_i^T s_i(t) \right) - H_i e_{d_i}(t) \right) \\ &\quad - \tilde{n}_i(t) \|H_i^T s_i(t)\| \end{aligned} \quad (26)$$

By applying straightforward calculations, it is obtained from (26) that

$$\begin{aligned} \dot{V}(t) \leq & -(m_i + \hat{n}_i) s_i^T(t) H_i \text{sat} \left( H_i^T s_i \right) \\ & + \left\| H_i^T s_i(t) \right\| \|\hat{n}_i\| \end{aligned} \quad (27)$$

The remaining steps of the proof follows from (21)–(23), which are omitted here for the sake of brevity. Therefore, the proof is now complete. ■

Thus, the reachability of the system trajectories into a region around the sliding surface is satisfied.

*Remark 3:* The controllers (19) and (24) are designed based on the utilization of the continuous function  $\text{sat} \left( H_i^T s_i(t) \right)$  with a guaranteed reachability condition. This approach effectively mitigates the chattering problem that often arises in practical implementations.

*Remark 4:* It is noted that current SMC approaches, such as those mentioned in [37], [45], are typically designed based on known upper bounds of disturbances. However, determining these bounds in practical applications can be challenging. In order to address this issue, in Corollary 1, the sliding mode controller is constructed in an adaptive manner without requiring prior knowledge of the upper bound of the estimated lumped disturbance and its first derivative. This demonstrates the applicability of the proposed controller for FC problems, even in situations where accurate knowledge of disturbance bounds is not readily available.

Next, the unknown parameters of the sliding surface, namely the controller gains  $K_i$  and  $K_{\tau_i}$ , can be determined using an equivalent control law. By considering (18), it follows that

$$\begin{aligned} \dot{s}_i(t) &= H_i \left( \dot{x}_i(t) - A_i x_i(t) - \hat{f}_i(t) \right) \\ &= H_i \left( B_i u_i(t) - B_i u_{s_i}(t) + f_i(t) - \hat{f}_i(t) \right) \\ &= u_i(t) + K_i x_i(t) - K_{\tau_i} x_i(t - \tau_i) + H_i f_i(t) \end{aligned} \quad (28)$$

Let  $\dot{s}_i(t) = 0$ , we then derive the equivalent control law as follows:

$$u_{eq_i}(t) = -K_i x_i(t) - K_{\tau_i} x_i(t - \tau_i) - H_i f_i(t) \quad (29)$$

Substituting (29) into (11), the sliding mode dynamics can be given as

$$\begin{aligned} \dot{x}_i(t) &= (A_i - B_i K_i) x_i(t) - B_i K_{\tau_i} x_i(t - \tau_i) + B_d f_i(t) \\ y_i(t) &= C_i x_i(t) \end{aligned} \quad (30)$$

where  $B_{d_i} = I_n - B_i H_i$ .

In the following analysis, it is assumed that  $K_{\tau_i}$  in (30) is a known parameter. Then, an LMI-based condition can be used to determine the unknown parameter  $K_i$  such that  $H_\infty$  performance requirement, as described in (17), is satisfied.

To begin, we define  $A_{d_i} = -B_i K_{\tau_i}$  and  $\bar{A}_i = A_i - B_i K_i$ . Then, (30) can be rewritten as

$$\begin{aligned} \dot{x}_i(t) &= \bar{A}_i x_i(t) + A_{d_i} x_i(t - \tau_i) + B_d f_i(t) \\ y_i(t) &= C_i x_i(t) \end{aligned} \quad (31)$$

Next, the following lemma is utilized for developing the subsequent theorem.

*Lemma 3 ([51]):* Consider  $X$  and  $Y$  as real constant matrices of appropriate dimensions. Then

$$X^T Y + Y^T X \leq \varepsilon X^T X + \frac{1}{\varepsilon} Y^T Y \quad (32)$$

holds for any  $\varepsilon > 0$ .

*Theorem 2:* Let  $\gamma_i$  be a given positive scalar. The sliding mode dynamics in (30) is globally asymptotically stable and meets the  $H_\infty$  performance requirement, if there exist symmetric, positive-definite matrices  $X_i$ ,  $Q_{1i}$ ,  $Q_{2i}$  and  $Q_{3i}$  such that the following inequality holds

$$\Theta_{d_i} = \begin{bmatrix} \Theta_{d_{i11}} & B_{d_i} & X_i C_i^T & \mathcal{A}_i \\ * & \Theta_{d_{i22}} & 0 & 0 \\ * & * & -I & 0 \\ * & * & * & -Q_i \end{bmatrix} < 0 \quad (33)$$

where

$$\begin{aligned} \Theta_{d_{i11}} &\triangleq \text{He} \left( (\bar{A}_i + A_{d_i}) X_i \right) + \tau_i A_{d_i} Q_{1i} A_{d_i}^T + \tau_i A_{d_i} Q_{2i} A_{d_i}^T, \\ \mathcal{A}_i &\triangleq \left[ X_i \bar{A}_i^T \quad X_i A_{d_i}^T \quad A_{d_i} \right], \\ \Theta_{d_{i22}} &\triangleq -\gamma_i^2 I + \tau_i B_{d_i}^T Q_{3i} B_{d_i}, \\ Q_i &\triangleq \text{diag} \left[ \frac{1}{\tau_i} Q_{1i}, \frac{1}{\tau_i} Q_{2i}, \frac{1}{\tau_i} Q_{3i} \right]. \end{aligned}$$

*Proof:* Consider  $x_i(t - \tau_i) = x_i(t) - \int_{t-\tau_i}^t \dot{x}_i(s) ds$ . Substituting (33) into the above formula yields

$$\begin{aligned} x_i(t - \tau_i) &= x_i(t) - A_{d_i} \int_{t-\tau_i}^t (\bar{A}_i x_i(s) \\ &\quad + A_{d_i} x_i(s - \tau_i) + B_d f_i(s)) ds \end{aligned} \quad (34)$$

We consider the following Lyapunov-Krasovskii Functional candidate:

$$V(x_i(t)) = V_0(x_i(t)) + V_1(x_i(t)) \quad (35)$$

where

$$\begin{aligned} V_0(x_i(t)) &= x_i^T(t) P_i x_i(t) \\ V_1(x_i(t)) &= \int_{-\tau_i}^0 \int_{t+\theta}^t x_i^T(s) \bar{A}_i^T Q_{1i}^{-1} \bar{A}_i x_i(s) ds d\theta \\ &\quad + \int_{-\tau_i}^0 \int_{t-\tau_i+\theta}^t x_i^T(s) A_{d_i}^T Q_{2i}^{-1} A_{d_i} x_i(s) ds d\theta \\ &\quad + \int_{-\tau_i}^0 \int_{t+\theta}^t d_i^T(s) B_{d_i}^T Q_{3i} B_{d_i} f_i(s) ds d\theta \end{aligned} \quad (36)$$

Differentiating (36) with respect to time along the trajectories of (34), yields

$$\begin{aligned} \dot{V}_0(x_i(t)) &= x_i^T(t) \left( P_i (\bar{A}_i + A_{d_i}) + (\bar{A}_i + A_{d_i})^T P_i \right) x_i(t) \\ &\quad - 2x_i^T(t) P_i A_{d_i} \left( \bar{A}_i \int_{t-\tau_i}^t x_i(s) ds + A_{d_i} \int_{t-\tau_i}^t x_i(s - \tau_i) ds \right) \end{aligned}$$

$$\begin{aligned}
 & + B_{d_i} \int_{t-\tau_i}^t f_i(s) ds \\
 & + 2x_i^T(t) P_i B_{d_i} f_i(t) \tag{37}
 \end{aligned}$$

Applying Lemma 2, we can obtain the following expressions, respectively:

$$\begin{aligned}
 & - 2x_i^T(t) P_i A_{d_i} \bar{A}_i \int_{t-\tau_i}^t x_i(s) ds \\
 & \leq \tau_i x_i^T(t) P_i A_{d_i} Q_{1i} A_{d_i}^T P_i x_i(t) \\
 & + \int_{t-\tau_i}^t x_i^T(s) \bar{A}_i^T Q_{1i}^{-1} \bar{A}_i x_i(s) ds \tag{38}
 \end{aligned}$$

$$\begin{aligned}
 & - 2x_i^T(t) P_i A_{d_i} \bar{A}_i \int_{t-\tau_i}^t x_i(s - \tau_i) ds \\
 & \leq \tau_i x_i^T(t) P_i A_{d_i} Q_{2i} A_{d_i}^T P_i x_i(t) \\
 & + \int_{t-\tau_i}^t x_i^T(s - \tau_i) A_{d_i}^T Q_{2i}^{-1} A_{d_i} x_i(s - \tau_i) ds \tag{39}
 \end{aligned}$$

$$\begin{aligned}
 & - 2x_i^T(t) P_i A_{d_i} B_i \int_{t-\tau_i}^t f_i(s) ds \\
 & \leq \tau_i x_i^T(t) P_i A_{d_i} Q_{3i}^{-1} A_{d_i}^T P_i x_i(t) \\
 & + \int_{t-\tau_i}^t f_i^T(s) B_{d_i}^T Q_{3i} B_{d_i} f_i(s) ds. \tag{40}
 \end{aligned}$$

Moreover, we have

$$\begin{aligned}
 \dot{V}_1(x_i(t)) & = \tau_i x_i^T(t) \bar{A}_i^T Q_{1i}^{-1} \bar{A}_i x_i(t) \\
 & - \int_{t-\tau_i}^t x_i^T(s) \bar{A}_i^T Q_{1i}^{-1} \bar{A}_i x_i(s) ds \\
 & + \tau_i x_i^T(t) A_{d_i}^T Q_{2i}^{-1} A_{d_i} x_i(t) \\
 & - \int_{t-\tau_i}^t x_i^T(s - \tau_i) A_{d_i}^T Q_{2i}^{-1} A_{d_i} x_i(s - \tau_i) ds \\
 & + \tau_i d_i^T(t) B_{d_i}^T Q_{3i} B_{d_i} f_i(t) \\
 & - \int_{t-\tau_i}^t f_i^T(s) B_{d_i}^T Q_{3i} B_{d_i} f_i(s) ds \tag{41}
 \end{aligned}$$

Combining (38)–(41) gives

$$\begin{aligned}
 \dot{V}(x_i(t)) & \leq x_i^T(t) \left( P_i (\bar{A}_i + A_{d_i}) + (\bar{A}_i + A_{d_i})^T P_i \right) x_i(t) \\
 & + \tau_i x_i^T(t) \left( P_i A_{d_i} Q_{1i} A_{d_i}^T P_i + \bar{A}_i^T Q_{1i}^{-1} \bar{A}_i \right) x_i(t) \\
 & + \tau_i x_i^T(t) \left( P_i A_{d_i} Q_{2i} A_{d_i}^T P_i + A_{d_i}^T Q_{2i}^{-1} A_{d_i} \right) x_i(t) \\
 & + \tau_i x_i^T(t) P_i A_{d_i} Q_{3i}^{-1} A_{d_i}^T P_i x_i(t) \\
 & + 2x_i^T(t) P_i B_{d_i} f_i(t) \\
 & + \tau_i f_i^T(t) B_{d_i}^T Q_{3i} B_{d_i} f_i(t) \tag{42}
 \end{aligned}$$

The above inequality can be written in equivalent matrix form as:

$$\begin{aligned}
 \dot{V}(x_i(t)) & \leq \begin{bmatrix} x_i^T(t) & f_i^T(t) \end{bmatrix} \begin{bmatrix} \mathcal{M}_i & P_i B_{d_i} \\ * & \mathcal{T}_i \end{bmatrix} \begin{bmatrix} x_i(t) \\ f_i(t) \end{bmatrix} \tag{43}
 \end{aligned}$$

where

$$\mathcal{M}_i \triangleq P_i (\bar{A}_i + A_{d_i}) + (\bar{A}_i + A_{d_i})^T P_i$$

$$\begin{aligned}
 & + \tau_i \left( P_i A_{d_i} Q_{1i} A_{d_i}^T P_i + \bar{A}_i^T Q_{1i}^{-1} \bar{A}_i \right) \\
 & + \tau_i \left( P_i A_{d_i} Q_{2i} A_{d_i}^T P_i + A_{d_i}^T Q_{2i}^{-1} A_{d_i} \right) \\
 & + \tau_i \left( P_i A_{d_i} Q_{3i}^{-1} A_{d_i}^T P_i \right),
 \end{aligned}$$

$$\mathcal{T}_i \triangleq \tau_i B_{d_i}^T Q_{3i} B_{d_i}.$$

By examining (33), it is verified that

$$\begin{bmatrix} \Theta_{d_{i11}} & B_{d_i} & A_i \\ * & \mathcal{T}_i & 0 \\ * & * & Q_i \end{bmatrix} < 0 \tag{44}$$

Applying the Schur complement to (44) results in:

$$\begin{bmatrix} \mathcal{W}_i & B_{d_i} \\ * & \mathcal{T}_i \end{bmatrix} < 0 \tag{45}$$

where

$$\begin{aligned}
 \mathcal{W}_i & \triangleq (\bar{A}_i + A_{d_i}) X_i + X_i (\bar{A}_i + A_{d_i})^T \\
 & + \tau_i \left( A_{d_i} Q_{1i} A_{d_i}^T + X_i \bar{A}_i^T Q_{1i}^{-1} \bar{A}_i X_i \right) \\
 & + \tau_i \left( A_{d_i} Q_{2i} A_{d_i}^T + X_i A_{d_i}^T Q_{2i}^{-1} A_{d_i} X_i \right) \\
 & + \tau_i \left( A_{d_i} Q_{3i}^{-1} A_{d_i}^T \right)
 \end{aligned}$$

Then, pre-and post-multiplying (45) by  $\text{diag}(X_i^{-1}, I)$  and defining  $P_i = X_i^{-1}$  gives

$$\begin{bmatrix} \mathcal{M}_i & P_i B_{d_i} \\ * & \mathcal{T}_i \end{bmatrix} < 0 \tag{46}$$

From (46), it is clear that  $\dot{V}(x_i(t)) < 0$ , which proves that the system (31) is internally stable. In the next step, we define the following performance function:

$$J_{T_i} = \int_0^T \left( y_i^T(t) y_i(t) - \gamma_i^2 f_i^T(t) f_i(t) \right) dt \tag{47}$$

Noticing that

$$\begin{aligned}
 J_{T_i} & = \int_0^T \left( y_i^T(t) y_i(t) - \gamma_i^2 f_i^T(t) f_i(t) + \dot{V}(x_i(t)) \right) dt \\
 & - \int_0^T \dot{V}(x_i(t)) dt \\
 & = \int_0^T \left( y_i^T(t) y_i(t) - \gamma_i^2 f_i^T(t) f_i(t) + \dot{V}(x_i(t)) \right) dt \\
 & - V(x_i(T)) \\
 & \leq \int_0^T \left( y_i^T(t) y_i(t) - \gamma_i^2 f_i^T(t) f_i(t) + \dot{V}(x_i(t)) \right) dt \tag{48}
 \end{aligned}$$

In view of (43), we obtain

$$\begin{aligned}
 & y_i^T(t) y_i(t) - \gamma_i^2 f_i^T(t) f_i(t) + \dot{V}(x_i(t)) \\
 & \leq \begin{bmatrix} x_i^T(t) & f_i^T(t) \end{bmatrix} \tilde{\Theta}_i \begin{bmatrix} x_i(t) \\ f_i(t) \end{bmatrix} \tag{49}
 \end{aligned}$$

$$\tilde{\Theta}_i = \begin{bmatrix} \tilde{\Theta}_{i11} & P_i B_{d_i} \\ * & \tilde{\Theta}_{i22} \end{bmatrix} \tag{50}$$

**TABLE 2.** Nominal quantities of the three-area power system [41], [46].

Area	$R_i$	$T_{G_i}$	$T_{T_i}$	$K_{P_i}$	$T_{P_i}$	$q_{ij}$	$K_{B_i}$	$T_{B_i}$
1	2.41	0.08	0.31	121	20.5	0.55	4.5	0.03
2	2.73	0.072	0.34	112.5	26	0.65	5.4	0.034
3	2.52	0.07	0.35	116	20.5	0.545	6.2	0.037

where

$$\begin{aligned}\tilde{\Theta}_{i11} &\triangleq P_i (\bar{A}_i + A_{d_i}) + (\bar{A}_i + A_{d_i})^T P_i \\ &\quad + \tau_i P_i A_{d_i} Q_{1i} A_{d_i}^T P_i + \tau_i \bar{A}_i^T Q_{1i}^{-1} \bar{A}_i \\ &\quad + \tau_i P_i A_{d_i} Q_{2i} A_{d_i}^T P_i + \tau_i A_{d_i}^T Q_{2i}^{-1} A_{d_i} \\ &\quad + \tau_i P_i A_{d_i} Q_{3i}^{-1} A_{d_i}^T P_i + C_i^T C_i, \\ \tilde{\Theta}_{i22} &\triangleq -\gamma_i^2 I + T_i.\end{aligned}$$

Let  $X_i = P_i^{-1}$ . Pre- and post-multiplying (50) by  $\text{diag}\{X_i, I\}$  leads to

$$\begin{bmatrix} \mathcal{N}_{11} & B_{d_i} \\ * & \tilde{\Theta}_{i22} \end{bmatrix} < 0 \quad (51)$$

where

$$\begin{aligned}\mathcal{N}_{11} &\triangleq (\bar{A}_i + A_{d_i}) X_i + X_i (\bar{A}_i + A_{d_i})^T \\ &\quad + \tau A_{d_i} Q_{1i} A_{d_i}^T + \tau_i X_i \bar{A}_i^T Q_{1i}^{-1} \bar{A}_i X_i \\ &\quad + \tau_i A_{d_i} Q_{2i} A_{d_i}^T + \tau_i X_i A_{d_i}^T Q_{2i}^{-1} A_{d_i} X_i \\ &\quad + \tau_i X_i A_{d_i} Q_{3i}^{-1} A_{d_i}^T X_i + X_i C_i^T C_i X_i\end{aligned}$$

Utilizing the Schur complement, the above inequality holds if and only if (33) is feasible. The above derivation shows that if the symmetric, positive-definite matrices  $X_i$ ,  $Q_{1i}$ ,  $Q_{2i}$  and  $Q_{3i}$ , then  $P_i = X_i^{-1} > 0$ , satisfying  $\tilde{\Theta}_i < 0$ , which means that  $J_{T_i} < 0$  for any  $T > 0$ . This completes the proof. ■

*Corollary 2:* Let  $\gamma_i$  be a given positive scalar, If there exist symmetric, positive-definite matrices  $X_i$ ,  $Q_{1i}$ ,  $Q_{2i}$ ,  $Q_{3i}$  and a matrix  $Y_i$  satisfying

$$\begin{bmatrix} \mathcal{H}_{11} & B_{d_i} & X_i C_i^T & \mathcal{H}_{14} \\ * & \tilde{\Theta}_{i22} & 0 & 0 \\ * & * & -I & 0 \\ * & * & * & -Q_i \end{bmatrix} < 0, \quad (52)$$

then the closed-loop system (31) with  $K_i = Y_i X_i^{-1}$  is stable and satisfies (17),

where

$$\begin{aligned}\mathcal{H}_{11} &\triangleq \text{He}((A_i + A_{d_i}) X_i - B_i Y_i) \\ &\quad + \tau_i A_{d_i} Q_{1i} A_{d_i}^T + \tau_i A_{d_i} Q_{2i} A_{d_i}^T, \\ \mathcal{H}_{14} &\triangleq [X_i A_i^T - Y_i^T B_i^T \quad X_i A_{d_i}^T \quad A_{d_i}].\end{aligned}$$

*Proof:* The proof follows from (33) by letting  $Y_i = K_i X_i$ . ■

## IV. SIMULATION RESULTS

In this section, three simulation cases are conducted to address the LFC problem in a three-area interconnected thermal power system with ESS cooperation, as depicted in Fig. 1. The performance of the designed controller compared with traditional PI and conventional SMC schemes is tested under various disturbances. The nominal system parameters for the three-area power system are presented in Table 2.

The tuning parameter  $L_i$  of the disturbance observer (13) is determined based on Lemma 2 and is chosen as an arbitrary positive definite matrix for all controlled areas. For the sake of simplicity, we assume:

$$L_i = \begin{bmatrix} 20 & 0 & 0 \\ 0 & 30 & 0 \\ 0 & 0 & 40 \end{bmatrix}$$

Appropriate values are also selected for the matrix gain  $K_{\tau_i}$ , the memory parameter  $\tau_i$  of the sliding surface (18) and the tuning parameter  $m_i$  of the proposed adaptive controller (24). In addition, the  $H_{\infty}$  performance index  $\gamma_i$  is minimized by solving the LMI constraint (52) using the YALMIP optimization toolbox [57]. This process determines the sliding surface gain  $K_i$ . A list of preset parameters and calculated values is provided in Table 3.

**Case 1:** In Case 1, the proposed MASMLFC is applied to the three-area power system with nominal parameters. The participation factors of the ESS and thermal power plan for all areas  $i = 1, 2, 3$  are assumed to be  $\chi_i = 0.3$  and  $\alpha_i = 0.7$ . A continuous nonlinear load variation of  $\Delta P_{L_1}(t) = 0.1 \times \text{Sin}(t)$  takes place in Area 1, followed by step load changes of  $\Delta P_{L_2}(t) = \Delta P_{L_3}(t) = 0.15$  p.u. in Areas 2 and 3 at  $t = 5$  s and at  $t = 15$  s, respectively. The dynamic performance of the proposed disturbance observer is shown in Fig. 3. The results demonstrate that the observer can estimate both the step and sinusoidal load perturbations, with the estimation error approaching zero after a short transient time. The system frequency deviation responses,  $\Delta f_i$ ,  $i = 1, 2, 3$ , under different control strategies, are illustrated in Fig. 4. The performance of the proposed MASMLFC is compared with SMLFC [34], DOB-SMLFC [60] and the conventional PI-based LFC. It can be observed that the proposed MASMLFC exhibits superior transient performance and significantly reduces frequency deviations compared to the other control strategies. A comparison of overshoot between the proposed MASMLFC (memory-based) and the DOB-SMLFC (memoryless) is provided in Table 4 for all three interconnected areas. Fig. 5 displays that the proposed scheme's sliding surface and control effort signals are smaller than those of the memory-less method in [60]. This indicates that the proposed scheme effectively eliminates the chattering effects by incorporating a saturation function in the design process. The system dynamics are driven to the sliding surfaces within finite time in all control areas. The impact of different memory parameters on the frequency deviation in Area2 is illustrated in Fig. 6. It can be observed that smaller memory parameters result

TABLE 3. Preset parameter values for the proposed sliding surface and adaptive controller.

Area	$\tau_i$	$m_i$	$\kappa_i$	$K_{\tau_i}$	$\gamma_i^{\min}$	$K_i$
1	0.8	0.1	0.01	$K_{\tau_1}=[3\ 0\ 0\ 0]$	0.4354	$K_1=[43.1101\ 31.5716\ 29.1974\ 2.1493]$
2	0.8	0.1	0.01	$K_{\tau_2}=[3\ 0\ 0\ 0]$	0.2123	$K_2=[75.0278\ 32.4739\ 30.0925\ 2.1028]$
3	0.8	0.1	0.01	$K_{\tau_3}=[3\ 0\ 0\ 0]$	0.3918	$K_3=[65.2439\ 37.6893\ 35.4081\ 2.0240]$

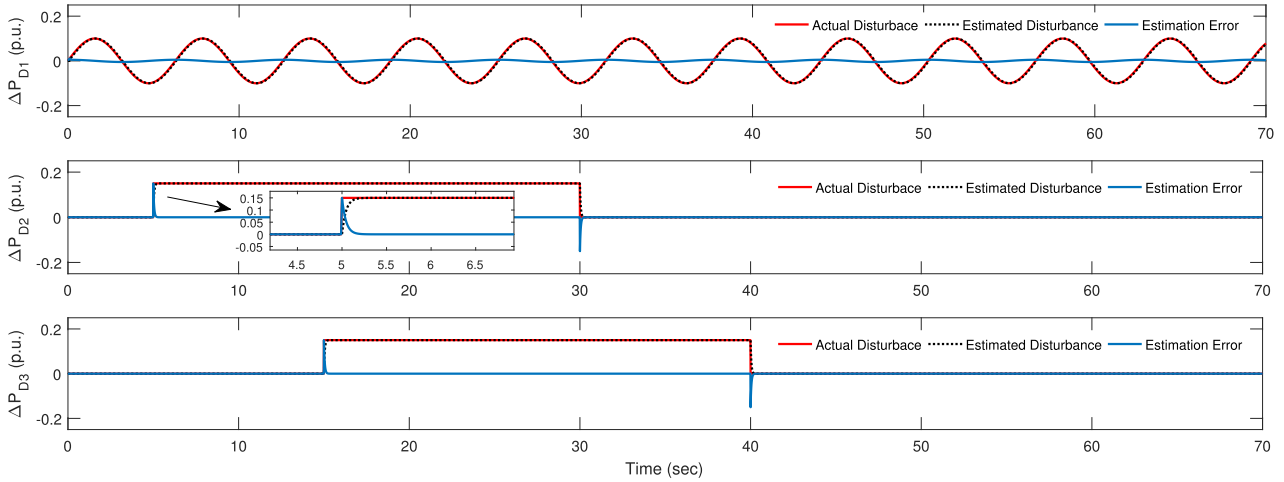


FIGURE 3. Disturbance estimation performance of the proposed DOB.

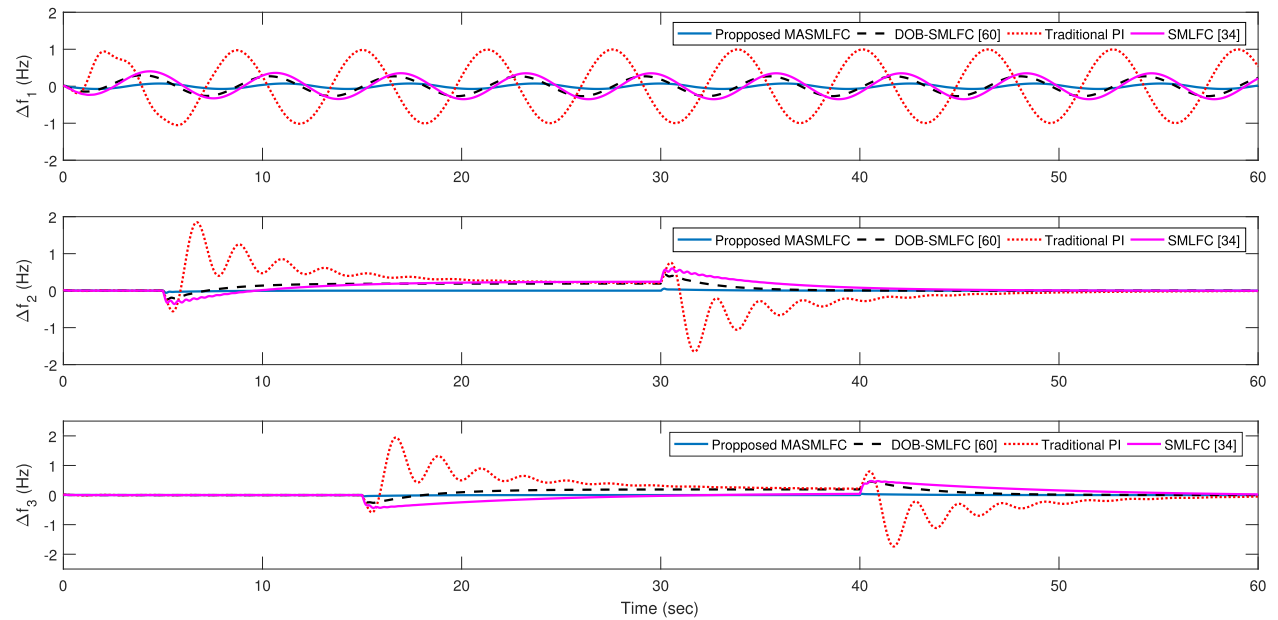


FIGURE 4. The frequency deviation responses with nominal plant parameters under different control strategies.

in increased overshoot and settling time. Thus, the proposed memory-based SMC method exhibits a great performance improvement on the transient response of the power system frequency deviations, thereby highlighting its advantages.

Case 2: In this subsection, the robustness of the proposed controller is evaluated under various uncertainties, including system parameter variations and nonlinear dynamics such as GRC limiters and GDB. In this simulation scenario,

a time-varying step load disturbance is applied to all three controlled areas, as shown in Fig. 7. Additionally, sine functions are used to simulate the bounded system parameter variations, with an uncertainty range of  $\pm 50\%$  around the nominal values given in Table 1. The GRC and GDB values are selected  $\pm 0.0018$  p.u.MW/sec and 0.6, respectively, for all three areas, based on [58]. The frequency deviation responses  $\Delta f_i$  for all control areas are shown in Fig. 8. It is evident from

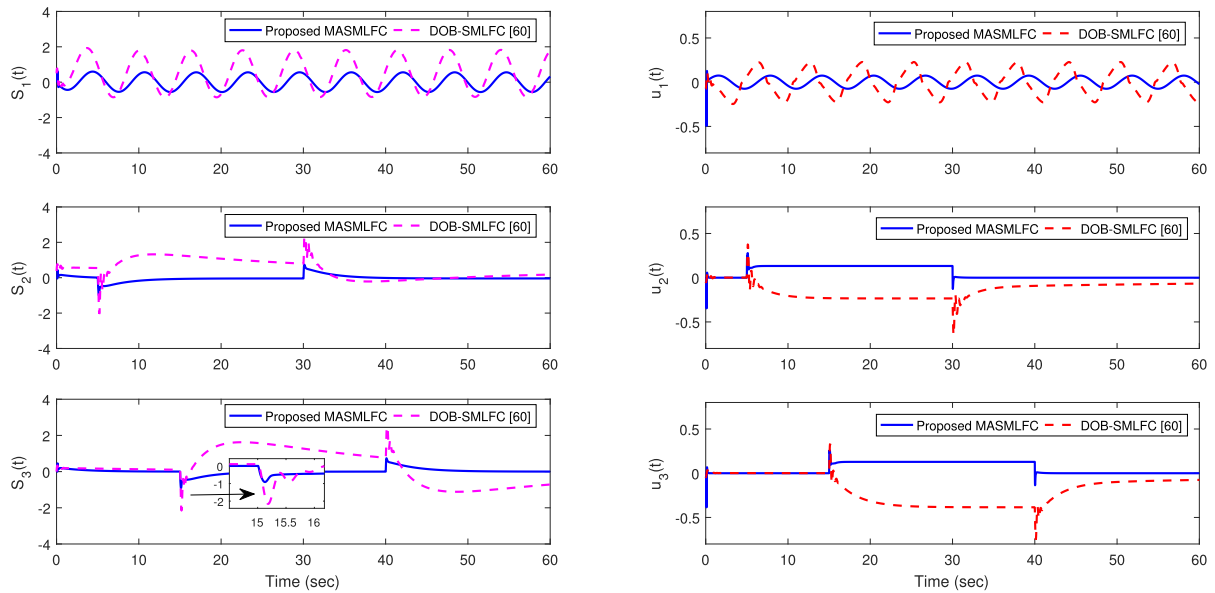


FIGURE 5. Comparative sliding surface  $s_i(t)$  and control effort  $u_i(t)$  between memory-based and memory-less approaches.

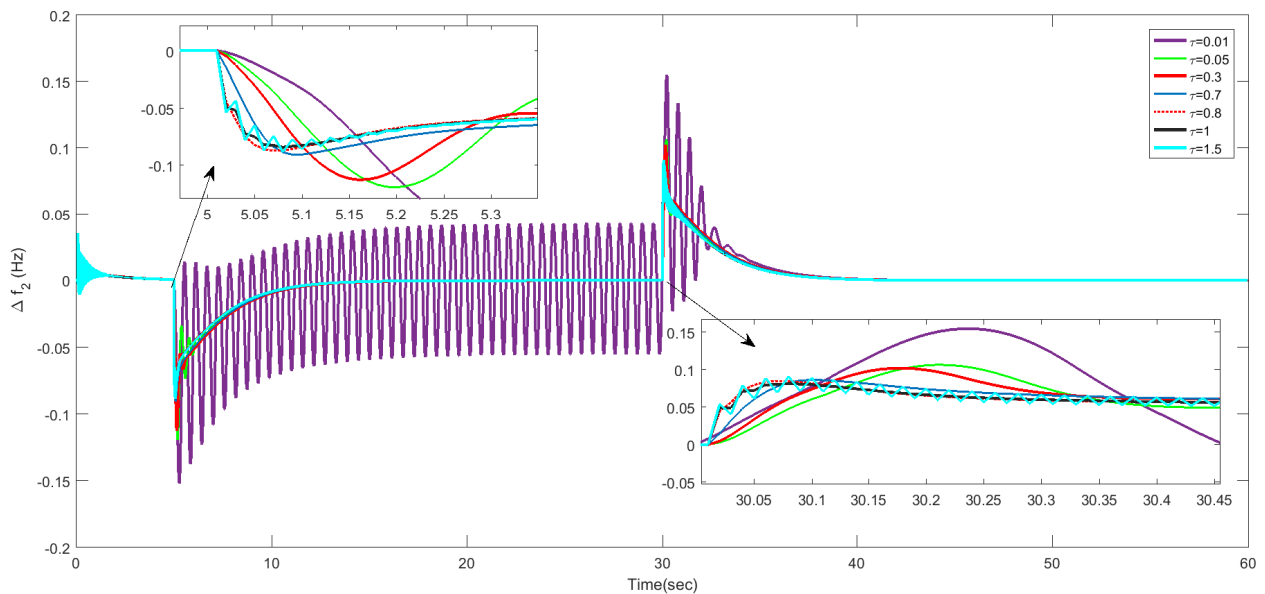


FIGURE 6. Frequency deviation response in area 2 under different memory parameters  $\tau_i$ .

Fig. 8 that the maximum values of frequency fluctuations with system parameter variations are  $|\Delta f_1|_{\max} = 0.16035$  Hz,  $|\Delta f_2|_{\max} = 0.1921$ , Hz  $|\Delta f_3|_{\max} = 0.2335$  Hz, whereas these values with GRC and GDB consideration increase by 0.2845, 0.3175 and 0.4545 Hz, respectively. The analysis indicates that the nonlinear dynamics, such as GRC limiters and GDB, have a more significant impact on the frequency deviations compared to system parameter variations. However, even in the presence of these nonlinear dynamics, the proposed controller, in conjunction with the ESS, effectively mitigates

the impact of these uncertainties on frequency deviations. This demonstrates the robust performance of the proposed controller under real operational conditions, where various uncertainties and nonlinearities are present.

Scenario 3: In Case 3, the effectiveness of the proposed control schemes is tested against a severe actual operating condition, where the power system disturbances are random and their bounds are unknown. Figs. 9 and 10 illustrate the bounded load and wind power fluctuations, respectively. The wind turbine parameters are listed in Table 5, and system

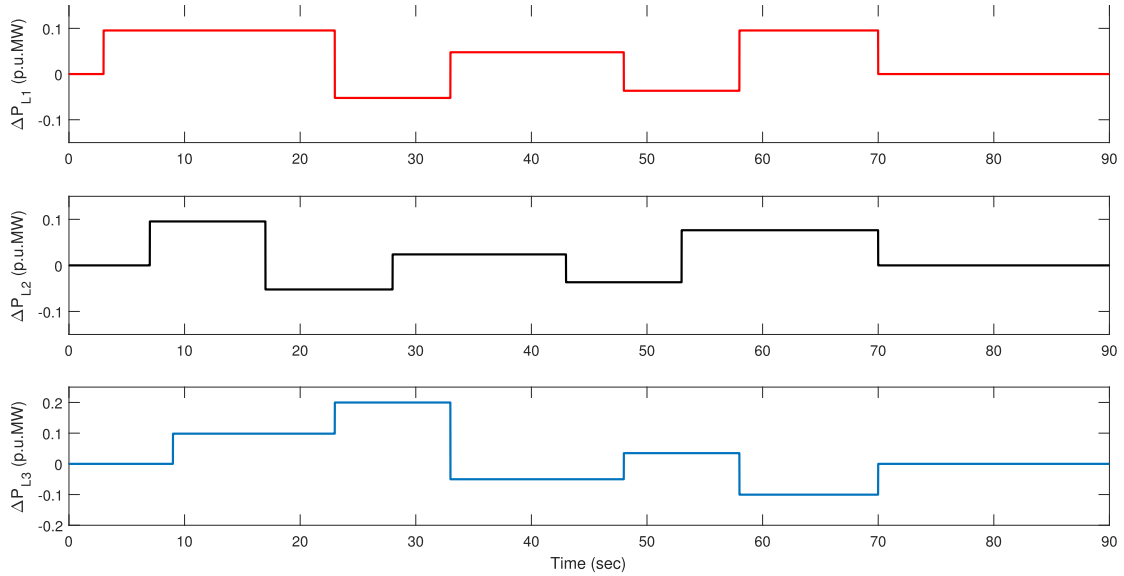


FIGURE 7. Variable step load disturbance pattern for all three areas.

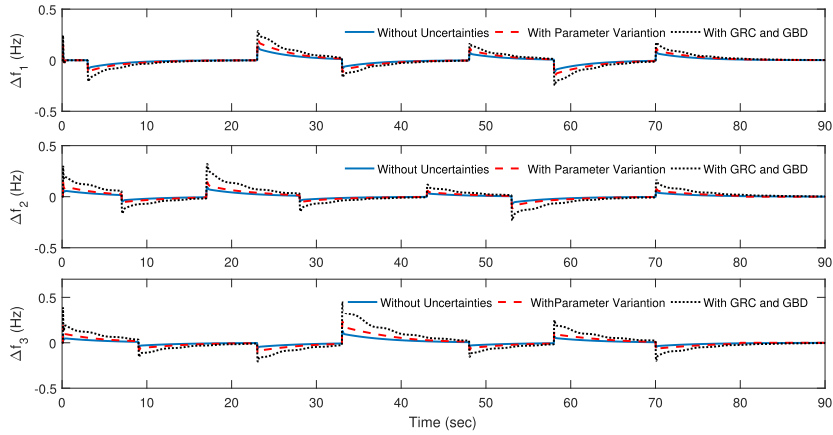


FIGURE 8. The frequency deviations response  $\Delta f_i$  under the proposed MASMLFC considering system parameter uncertainties with and without GRC and GDB nonlinearities.

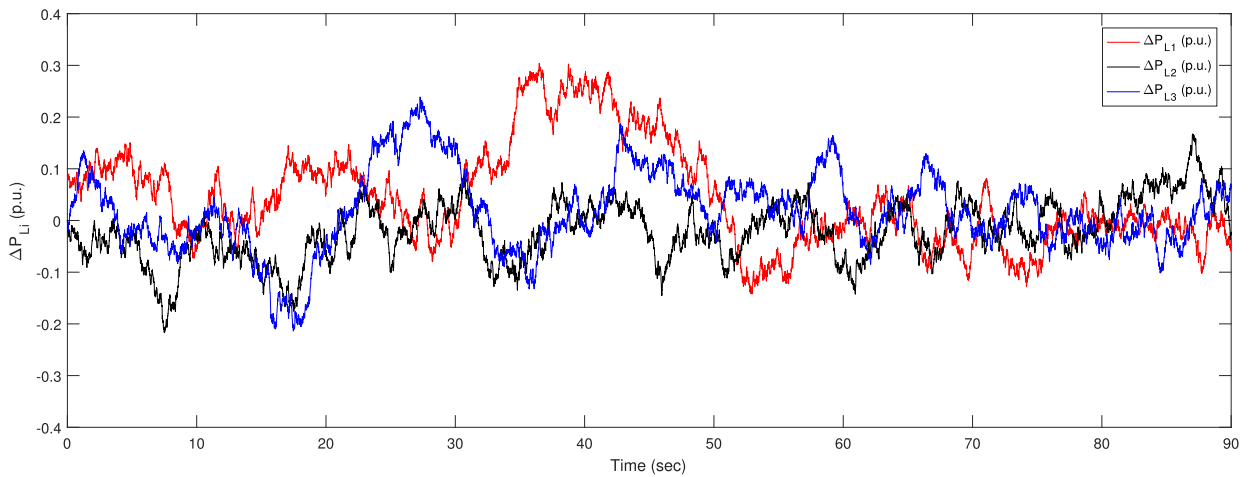


FIGURE 9. Random load profile for the three area interconnected power system.

parameter uncertainties remain the same in Case 2. In this simulation, the participation of ESS in the proposed LFC strategy is illustrated in Fig. 11. It is evident from Fig. 11

that the frequency nadir of the system in all controlled areas under ESS participation is decreased, and the dynamic response of the frequency deviations  $\Delta f_i$  exhibits improved

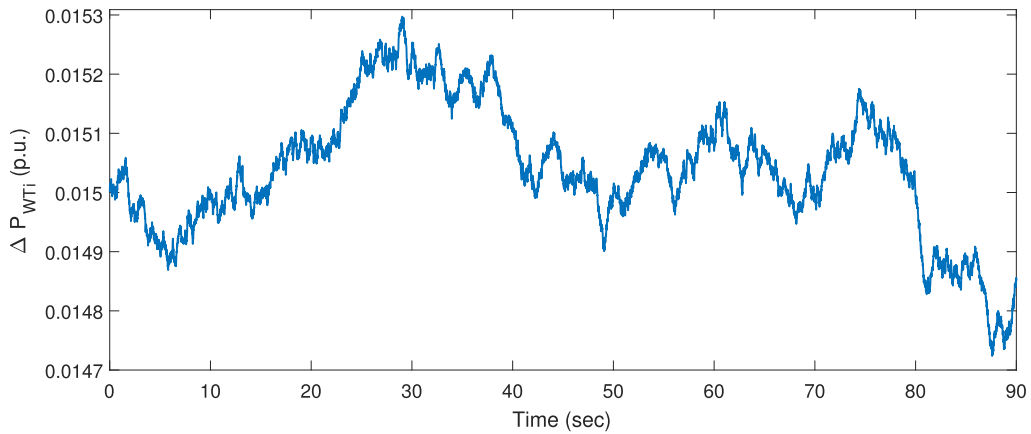


FIGURE 10. Wind power fluctuation profile.

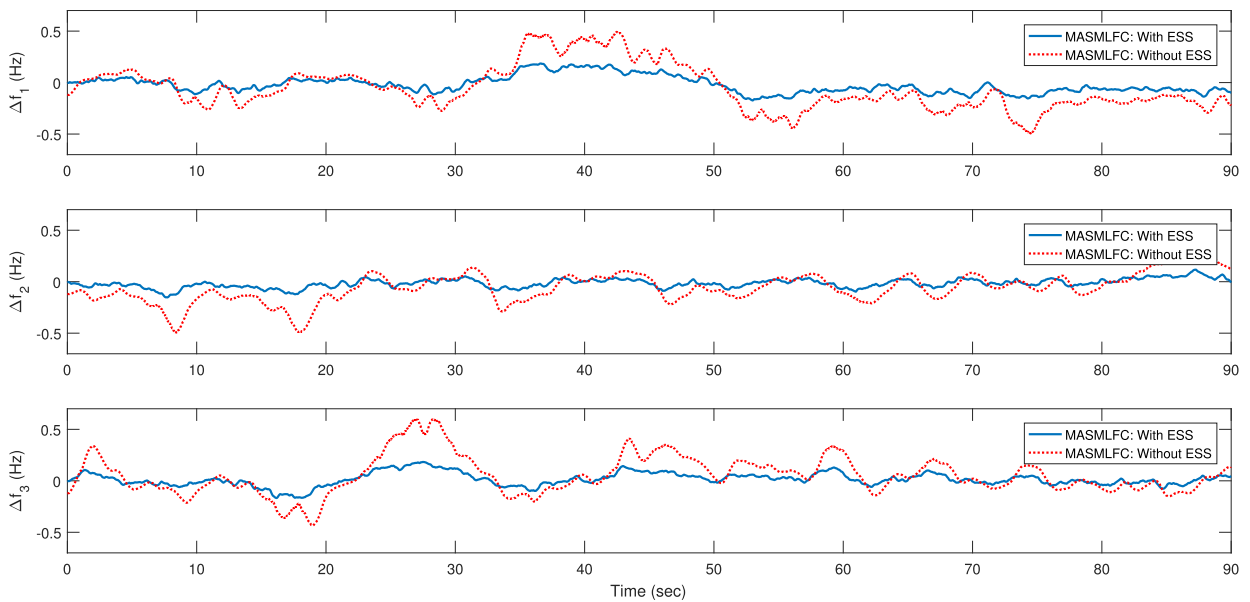


FIGURE 11. The frequency deviation responses with and without ESS participation under MASMLFC strategy with random disturbances.

TABLE 4. Comparative maximum frequency deviations.

Control Method	$ \Delta f_1 _{\max}$	$ \Delta f_2 _{\max}$	$ \Delta f_3 _{\max}$
DOB-SMLFC [60]	0.0924	0.1035	0.0987
Proposed MASMLFC	0.0773	0.0862	0.0825
Improvement	16.34%	16.71%	16.41%

$|\Delta f_i|_{\max}$ -Maximum frequency deviation in control area  $i = 1, 2, 3$

transient and steady-state performance compared to the case when ESS is not applied. This highlights the significance of effective coordination between the ESS and the proposed MASMLFC in maintaining the frequency deviations within an acceptable range and ensuring power system frequency stability. The simulation results presented in Fig. 12 highlight that the proposed approach demonstrates superior dynamic performance compared to other control strategies when

TABLE 5. Nominal parameters of the wind turbine [49], [50].

Area	$\rho_{w_i}$	$A_{w_{f_i}}$	$R_{blade}$	$\omega_{blade}$	$V_{w_i}$
1	1.225	1648	43.36	22.5	12
2	1.225	1648	43.36	22.5	12
3	1.225	1648	43.36	22.5	12

subjected to both random matched and mismatched disturbances arising from system parameter variations, load changes and wind power fluctuations. Additionally, the performance indicators shown in Table 6 provide further evidence of the superior performance of the proposed MASMLFC strategy compared to the other approaches in terms of minimizing the influence of random disturbances on the controlled output  $\Delta f_i$ . This confirms the robustness of the designed controller in mitigating the effects of random disturbances and maintaining desired system performance.

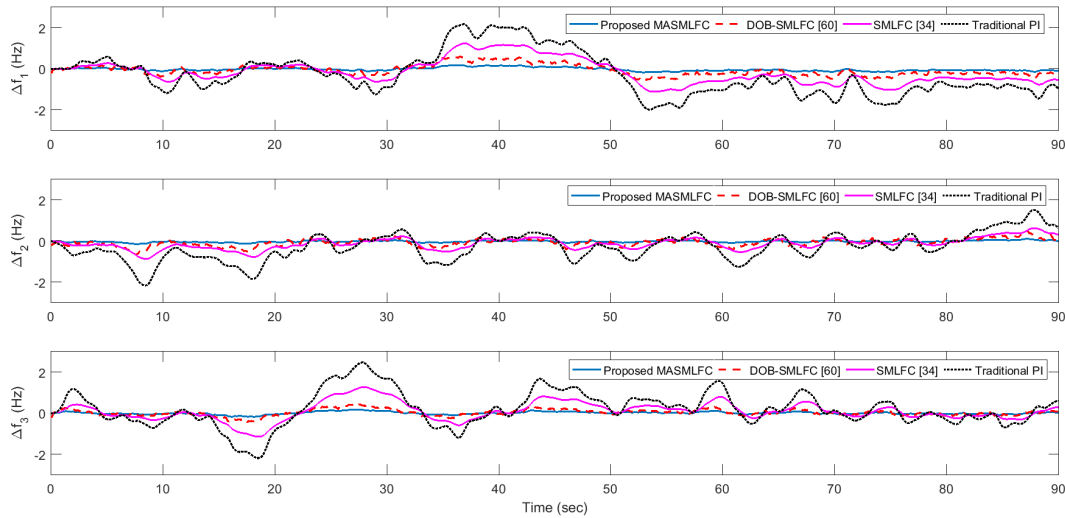


**FIGURE 12.** The frequency deviation responses in all three interconnected areas under various LFC methods considering random disturbances.

**TABLE 6.** Performance indices across all controlled areas.

LFC Scheme	ISE			IAE			ITAE		
	Control Area								
	1	2	3	1	2	3	1	2	3
Proposed MASMLFC	0.0046	0.0018	0.0076	0.1104	0.0709	0.1797	4.1692	2.9610	5.7756
DOB-SMLFC [60]	0.03117	0.0083	0.0542	0.2347	0.1903	0.2860	7.6505	4.9201	9.5918
SMLFC [34]	0.1410	0.0623	0.1683	0.7078	0.6103	0.7926	22.5099	13.8784	29.5164
Traditional PI	1.3003	0.9834	1.7813	6.0699	5.1042	7.1643	99.7801	80.5310	138.4906

**V. CONCLUSION**

The proposed paper introduces a memory-based adaptive sliding mode LFC scheme for multiarea interconnected power systems with ESS. The system’s dynamic model is developed, and a disturbance observer is developed to accurately estimate the lumped disturbance. The sliding surface design incorporates current and delayed state variables along with the estimated disturbance to improve the dynamic performance of the controller. An  $H_\infty$ -based sliding mode controller utilizing rigorous LMIs is constructed. A detailed synthesis analysis is conducted to validate the theoretical properties of the proposed control strategy. The simulation results demonstrate that the proposed MASMLFC method outperforms the recent memoryless SMC approaches in terms of transient performance for the LFC problem. The selection of an appropriate memory parameter  $\tau_i$  enhances the controller’s transient response. The continuous control law also contributes to reducing chattering and control effort, as observed in the simulation results. The proposed controller exhibits robust performance in the presence of random uncertainties and unmodeled dynamics. Furthermore, the coordination of MASMLFC with energy storage devices effectively mitigates frequency deviations caused by large power perturbations, thereby reducing mechanical stress on the traditional thermal units and improving power system frequency stability.

Considering the promising results of the proposed approach, our future work will focus on deriving a fuzzy-evolutionary optimization algorithm to cooperatively determine the memory parameter of the sliding surface and the variable gain of the ESS, subject to the state of charge constraints. Additionally, with the growing integration of renewable energy sources and ESS in future power system configurations, it becomes imperative to explore the suitability of employing of the sliding mode control strategy in smart grids for hybrid power systems that face communication delays.

**CREDIT AUTHORSHIP CONTRIBUTION STATEMENT**

Farhad Farivar: conceptualization, methodology, software, validation, formal analysis. Octavian Bass: supervision, methodology, writing—review and editing. Daryoush Habibi: supervision, methodology, writing—review and editing.

**DECLARATION OF COMPETING INTERESTS**

The authors declare that they have no known competing financial interests or personal relationships that could have appeared to influence the work reported in this paper.

**REFERENCES**

[1] P. Kundur, *Power System Stability and Control*. New York, NY, USA: McGraw-Hill, 1994.

- [2] S. K. Pandey, S. R. Mohanty, and N. Kishor, "A literature survey on load-frequency control for conventional and distribution generation power systems," *Renew. Sustain. Energy Rev.*, vol. 25, pp. 318–334, Sep. 2013.
- [3] H. Bevrani, *Robust Power System Frequency Control*. New York, NY, USA: Springer, 2009.
- [4] L. Dong, Y. Zhang, and Z. Gao, "A robust decentralized load frequency controller for interconnected power systems," *ISA Trans.*, vol. 51, no. 3, pp. 410–419, May 2012.
- [5] C. K. Das, O. Bass, G. Kothapalli, T. S. Mahmoud, and D. Habibi, "Overview of energy storage systems in distribution networks: Placement, sizing, operation, and power quality," *Renew. Sustain. Energy Rev.*, vol. 91, pp. 1205–1230, Aug. 2018.
- [6] D. Wang, L. Liu, H. Jia, W. Wang, Y. Zhi, Z. Meng, and B. Zhou, "Review of key problems related to integrated energy distribution systems," *CSEE J. Power Energy Syst.*, vol. 4, no. 2, pp. 130–145, Jun. 2018.
- [7] M. Elsis, N. Bazmohammadi, J. M. Guerrero, and M. A. Ebrahim, "Energy management of controllable loads in multi-area power systems with wind power penetration based on new supervisor fuzzy nonlinear sliding mode control," *Energy*, vol. 221, Apr. 2021, Art. no. 119867.
- [8] K. Naidu, H. Mokhlis, and A. H. A. Bakar, "Multiobjective optimization using weighted sum artificial bee colony algorithm for load frequency control," *Int. J. Electr. Power Energy Syst.*, vol. 55, pp. 657–667, Feb. 2014.
- [9] M. Elsis, M. Aboelela, M. Soliman, and W. Mansour, "Design of optimal model predictive controller for LFC of nonlinear multi-area power system with energy storage devices," *Electr. Power Compon. Syst.*, vol. 46, nos. 11–12, pp. 1300–1311, Jul. 2018.
- [10] T. H. Mohamed, M. A. M. Alamin, and A. M. Hassan, "A novel adaptive load frequency control in single and interconnected power systems," *Ain Shams Eng. J.*, vol. 12, no. 2, pp. 1763–1773, Jun. 2021.
- [11] H. Yousef, "Adaptive fuzzy logic load frequency control of multi-area power system," *Int. J. Electr. Power Energy Syst.*, vol. 68, pp. 384–395, Jun. 2015.
- [12] D. Xu, J. Liu, X.-G. Yan, and W. Yan, "A novel adaptive neural network constrained control for a multi-area interconnected power system with hybrid energy storage," *IEEE Trans. Ind. Electron.*, vol. 65, no. 8, pp. 6625–6634, Aug. 2018.
- [13] N. Hasan, I. Nasiruddin, P. Kumar, and N. Hakimuddin, "Sub-optimal automatic generation control of interconnected power system using constrained feedback control strategy," *Int. J. Electr. Power Energy Syst.*, vol. 43, no. 1, pp. 295–303, Dec. 2012.
- [14] H. Bevrani, Y. Mitani, and K. Tsuji, "Robust decentralised load-frequency control using an iterative linear matrix inequalities algorithm," *IEE Proc., Gener. Transmiss. Distrib.*, vol. 151, no. 3, pp. 347–354, May 2004.
- [15] K. Lu, W. Zhou, G. Zeng, and Y. Zheng, "Constrained population extremal optimization-based robust load frequency control of multi-area interconnected power system," *Int. J. Electr. Power Energy Syst.*, vol. 105, pp. 249–271, Feb. 2019.
- [16] O. P. Malik, A. Kumar, and G. S. Hope, "A load frequency control algorithm based on a generalized approach," *IEEE Trans. Power Syst.*, vol. 3, no. 2, pp. 375–382, May 1988.
- [17] K. R. M. V. Chandrakala, S. Balamurugan, and K. Sankaranarayanan, "Variable structure fuzzy gain scheduling based load frequency controller for multi source multi area hydro thermal system," *Int. J. Electr. Power Energy Syst.*, vol. 53, pp. 375–381, Dec. 2013.
- [18] Y. Zheng, Z. Chen, Z. Huang, M. Sun, and Q. Sun, "Active disturbance rejection controller for multi-area interconnected power system based on reinforcement learning," *Neurocomputing*, vol. 425, pp. 149–159, Feb. 2021.
- [19] H. Li, X. Wang, and J. Xiao, "Adaptive event-triggered load frequency control for interconnected microgrids by observer-based sliding mode control," *IEEE Access*, vol. 7, pp. 68271–68280, 2019.
- [20] Z. Wu, H. Mo, J. Xiong, and M. Xie, "Adaptive event-triggered observer-based output feedback  $L_\infty$  load frequency control for networked power systems," *IEEE Trans. Ind. Informat.*, vol. 16, no. 6, pp. 3952–3962, Jun. 2020.
- [21] H. Shayeghi, H. A. Shayanfar, and A. Jalili, "Load frequency control strategies: A state-of-the-art survey for the researcher," *Energy Convers. Manage.*, vol. 50, no. 2, pp. 344–353, Feb. 2009.
- [22] R. Shankar, S. R. Pradhan, K. Chatterjee, and R. Mandal, "A comprehensive state of the art literature survey on LFC mechanism for power system," *Renew. Sustain. Energy Rev.*, vol. 76, pp. 1185–1207, Sep. 2017.
- [23] V. I. Utkin and H.-C. Chang, "Sliding mode control on electro-mechanical systems," *Math. Problems Eng.*, vol. 8, nos. 4–5, pp. 451–473, Jan. 2002.
- [24] J. Hu, H. Zhang, H. Liu, and X. Yu, "A survey on sliding mode control for networked control systems," *Int. J. Syst. Sci.*, vol. 52, no. 6, pp. 1129–1147, Apr. 2021.
- [25] J. Guo, "Application of full order sliding mode control based on different areas power system with load frequency control," *ISA Trans.*, vol. 92, pp. 23–34, Sep. 2019.
- [26] D. Qian, S. Tong, H. Liu, and X. Liu, "Load frequency control by neural-network-based integral sliding mode for nonlinear power systems with wind turbines," *Neurocomputing*, vol. 173, pp. 875–885, Jan. 2016.
- [27] C. Mu, Y. Tang, and H. He, "Improved sliding mode design for load frequency control of power system integrated an adaptive learning strategy," *IEEE Trans. Ind. Electron.*, vol. 64, no. 8, pp. 6742–6751, Aug. 2017.
- [28] J. Guo, "The load frequency control by adaptive high order sliding mode control strategy," *IEEE Access*, vol. 10, pp. 25392–25399, 2022.
- [29] A. Bagheri, A. Jabbari, and S. Mobayen, "An intelligent ABC-based terminal sliding mode controller for load-frequency control of islanded micro-grids," *Sustain. Cities Soc.*, vol. 64, Jan. 2021, Art. no. 102544.
- [30] V. Utkin and J. Shi, "Integral sliding mode in systems operating under uncertainty conditions," in *Proc. 35th IEEE Conf. Decis. Control*, Koba, Japan, Dec. 1996, pp. 4591–4596.
- [31] Q. Hu, "Robust integral variable structure controller and pulse-width pulse-frequency modulated input shaper design for flexible spacecraft with mismatched uncertainty/disturbance," *ISA Trans.*, vol. 46, no. 4, pp. 505–518, Oct. 2007.
- [32] S. Prasad, S. Purwar, and N. Kishor, "Non-linear sliding mode load frequency control in multi-area power system," *Control Eng. Pract.*, vol. 61, pp. 81–92, Apr. 2017.
- [33] K. Vrdoljak, N. Perić, and I. Petrović, "Sliding mode based load-frequency control in power systems," *Electr. Power Syst. Res.*, vol. 80, no. 5, pp. 514–527, May 2010.
- [34] Y. Mi, Y. Fu, C. Wang, and P. Wang, "Decentralized sliding mode load frequency control for multi-area power systems," *IEEE Trans. Power Syst.*, vol. 28, no. 4, pp. 4301–4309, Nov. 2013.
- [35] Y.-S. Lu and C.-W. Chiu, "A stability-guaranteed integral sliding disturbance observer for systems suffering from disturbances with bounded first time derivatives," *Int. J. Control, Autom. Syst.*, vol. 9, no. 2, pp. 402–409, Apr. 2011.
- [36] M. Chen and W.-H. Chen, "Sliding mode control for a class of uncertain nonlinear system based on disturbance observer," *Int. J. Adapt. Control Signal Process.*, vol. 24, no. 1, pp. 51–64, Jan. 2010.
- [37] Y. Mi, Y. Fu, D. Li, C. Wang, P. C. Loh, and P. Wang, "The sliding mode load frequency control for hybrid power system based on disturbance observer," *Int. J. Electr. Power Energy Syst.*, vol. 74, pp. 446–452, Jan. 2016.
- [38] J. Yang, S. Li, and X. Yu, "Sliding-mode control for systems with mismatched uncertainties via a disturbance observer," *IEEE Trans. Ind. Electron.*, vol. 60, no. 1, pp. 160–169, Jan. 2013.
- [39] W.-H. Chen, J. Yang, L. Guo, and S. Li, "Disturbance-observer-based control and related methods—An overview," *IEEE Trans. Ind. Electron.*, vol. 63, no. 2, pp. 1083–1095, Feb. 2016.
- [40] Z. Wang and Y. Liu, "Adaptive terminal sliding mode based load frequency control for multi-area interconnected power systems with PV and energy storage," *IEEE Access*, vol. 9, pp. 120185–120192, 2021.
- [41] I. Ngamroo and S. Vachirasricirikul, "Design of optimal SMES controller considering SOC and robustness for microgrid stabilization," *IEEE Trans. Appl. Supercond.*, vol. 26, no. 7, pp. 1–5, Oct. 2016.
- [42] K. Liao and Y. Xu, "A robust load frequency control scheme for power systems based on second-order sliding mode and extended disturbance observer," *IEEE Trans. Ind. Informat.*, vol. 14, no. 7, pp. 3076–3086, Jul. 2018.
- [43] H. H. Alhelou, N. Nagpal, N. Kassarwani, and P. Siano, "Decentralized optimized integral sliding mode-based load frequency control for interconnected multi-area power systems," *IEEE Access*, vol. 11, pp. 32296–32307, 2023.
- [44] F. Yang, X. Shao, S. M. Mueen, D. Li, S. Lin, and C. Fang, "Disturbance observer based fractional-order integral sliding mode frequency control strategy for interconnected power system," *IEEE Trans. Power Syst.*, vol. 36, no. 6, pp. 5922–5932, Nov. 2021.

- [45] Y. Mi, X. Hao, Y. Liu, Y. Fu, C. Wang, P. Wang, and P. C. Loh, "Sliding mode load frequency control for multi-area time-delay power system with wind power integration," *IET Gener., Transmiss. Distrib.*, vol. 11, no. 18, pp. 4644–4653, Dec. 2017.
- [46] S. Prasad, S. Purwar, and N. Kishor, "Load frequency regulation using observer based non-linear sliding mode control," *Int. J. Electr. Power Energy Syst.*, vol. 104, pp. 178–193, Jan. 2019.
- [47] Y. Cui, L. Xu, M. Fei, and Y. Shen, "Observer based robust integral sliding mode load frequency control for wind power systems," *Control Eng. Pract.*, vol. 65, pp. 1–10, Aug. 2017.
- [48] L. Cai, Z. He, and H. Hu, "A new load frequency control method of multi-area power system via the viewpoints of port-Hamiltonian system and cascade system," *IEEE Trans. Power Syst.*, vol. 32, no. 3, pp. 1689–1700, May 2017.
- [49] D.-J. Lee and L. Wang, "Small-signal stability analysis of an autonomous hybrid renewable energy power generation/energy storage system. Part I: Time-domain simulations," *IEEE Trans. Energy Convers.*, vol. 23, no. 1, pp. 311–320, Mar. 2008.
- [50] G. Magdy, E. A. Mohamed, G. Shabib, A. A. Elbaset, and Y. Mitani, "SMES based a new PID controller for frequency stability of a real hybrid power system considering high wind power penetration," *IET Renew. Power Gener.*, vol. 12, no. 11, pp. 1304–1313, Aug. 2018.
- [51] S. Boyd, L. E. Ghaoui, E. Feron, and V. Balakrishnan, *Linear Matrix Inequalities in System and Control Theory*. Philadelphia, PA, USA: SIAM, 1994.
- [52] A. Ahmadi and M. Aldeen, "An LMI approach to the design of robust delay-dependent overlapping load frequency control of uncertain power systems," *Int. J. Electr. Power Energy Syst.*, vol. 81, pp. 48–63, Oct. 2016.
- [53] L. Xiong, H. Li, and J. Wang, "LMI based robust load frequency control for time delayed power system via delay margin estimation," *Int. J. Electr. Power Energy Syst.*, vol. 100, pp. 91–103, Sep. 2018.
- [54] D. Rerkpreedapong, A. Hasanovic, and A. Feliachi, "Robust load frequency control using genetic algorithms and linear matrix inequalities," *IEEE Trans. Power Syst.*, vol. 18, no. 2, pp. 855–861, May 2003.
- [55] G.-R. Duan and H.-H. Yu, *LMIs in Control Systems: Analysis, Design and Applications*. Boca Raton, FL, USA: CRC Press, 2013.
- [56] P. Haghghi, B. Tavassoli, and A. Farhadi, "A practical approach to networked control design for robust  $H_\infty$  performance in the presence of uncertainties in both communication and system," *Appl. Math. Comput.*, vol. 381, Sep. 2020, Art. no. 125308.
- [57] J. Löfberg, "Automatic robust convex programming," *Optim. Methods Softw.*, vol. 27, no. 1, pp. 115–129, Feb. 2012.
- [58] P. Bhui, N. Senroy, A. K. Singh, and B. C. Pal, "Estimation of inherent governor dead-band and regulation using unscented Kalman filter," *IEEE Trans. Power Syst.*, vol. 33, no. 4, pp. 3546–3558, Jul. 2018.
- [59] H. Khalil, *Nonlinear Control*. New York, NY, USA: Pearson, 2015.
- [60] F. Farivar, O. Bass, and D. Habibi, "Decentralized disturbance observer-based sliding mode load frequency control in multiarea interconnected power systems," *IEEE Access*, vol. 10, pp. 92307–92320, 2022.



research interest includes applications of control theories in power systems.

**FARHAD FARIVAR** (Graduate Student Member, IEEE) received the B.S. degree in electrical power systems from Azad University, Iran, in 2006, and the M.Eng. degree in instrumentation, control, and automation from Edith Cowan University, Joondalup, WA, Australia, in 2014, where he is currently pursuing the Ph.D. degree with the Smart Energy Systems Group. Since 2014, he has been a Senior Electrical Engineer with the School of Engineering, Edith Cowan University. His main



from 2006 to 2009. He is currently a Senior Lecturer with the School of Engineering, Edith Cowan University, Perth, WA, Australia. He has coauthored 90 professional publications. His research interests include smart grid technologies, renewable energy resources, and nonlinear dynamics in power electronic.

**OCTAVIAN BASS** (Senior Member, IEEE) received the bachelor's and Ph.D. degrees from the Politehnica University of Timisoara, Romania, in 1995 and 2001, respectively. His employment history includes research positions with the Budapest University of Technology and Economics, Hungary; The Hong Kong Polytechnic University; Hull University, U.K.; and Utsunomiya University, Japan. He was a Lecturer with James Cook University, Australia,



his research interests include engineering design for sustainable development, reliability and quality of service in communication systems and networks, smart energy systems, and environmental monitoring technologies. He is a fellow of Engineers Australia and the Institute of Marine Engineering, Science and Technology.

**DARYOUSH HABIBI** (Senior Member, IEEE) received the B.E. (Hons.) and Ph.D. degrees in electrical engineering from the University of Tasmania, Hobart, Australia, in 1989 and 1994, respectively. His employment history includes Telstra Research Laboratories, Flinders University, Intelligent Pixels Inc., and Edith Cowan University, Joondalup, WA, Australia, where he is currently a Professor, a Pro Vice-Chancellor, and the Executive Dean of the School of Engineering. His

• • •